



An actual thermal efficiency expression for heat engines: Effect of heat transfer roadmaps



Jinliang Xu ^{a,*}, Yawen Zheng ^a, Yanjuan Wang ^a, Xufei Yang ^a, Chao Yu ^a, Xuewang Xie ^b, Zhi Li ^b, Xiaoli Zhao ^b

^aThe Beijing Key Laboratory of Multiphase Flow and Heat Transfer for Low Grade Energy Utilization, North China Electric Power University, Beijing 102206, PR China

^bHebei Electric Power Design & Research Institute, Shijiazhuang 050031, Hebei, PR China

ARTICLE INFO

Article history:

Received 24 March 2017

Received in revised form 20 May 2017

Accepted 26 May 2017

Keywords:

Heat engine

Heat transfer

Thermodynamics

Dissipation

Thermal efficiency

ABSTRACT

In the framework of modern thermodynamics, “thermodynamics flow” and “thermodynamics force” are introduced to develop a real thermal efficiency expression for heat engine, which receives heat from a heat source and dissipates heat to environment to yield a work output, for the first time. Enclosed area of T - Q curves of a counter-current heat exchanger is the dissipation for heat to power conversion, representing loss of thermal energy quality. The relationship between heat load and dissipation for heat to power conversion is quantified. Such connection is written for both heating and cooling processes. Linking the thermal couplings between heating and cooling processes yields the thermal efficiency expressed as $\eta_{real} = C\eta_{Carnot}$, where $C = \frac{1}{\eta_{Carnot}} - \frac{R}{1-\eta_{Carnot}}$, η_{Carnot} is the Carnot efficiency, $R = R_h/R_c$ is the ratio of resistance in heating process R_h divided by that in cooling process R_c . The thermal efficiency theory tells us that no matter how complex a heat engine is, the engine should reach a lower resistance ratio of heating process with respect to cooling process to raise its thermal efficiency. The guidelines for design and operation of general heat engines are provided. A link between heat transfer and thermodynamics is presented in this work. As an application example, the effect of critical temperatures of organic fluids on the performance of Organic Rankine Cycles is successfully explained by the newly developed theory.

© 2017 Elsevier Ltd. All rights reserved.

1. Introduction

Carnot theorem is the foundation stone of thermodynamics and the starting point of the second law of thermodynamics. Carnot theorem states that the efficiency of a reversible heat engine is the highest. Carnot theorem emphasized “reversibility” of Carnot cycle, and resulted in the establishment of thermodynamics for reversible and irreversible processes in classical thermodynamics. Now it has been found that the general necessary and sufficient condition for the highest conversion efficiency of energy is “non-dissipation” but not “reversibility” of process or system [1]. This is the extended Carnot theorem. A non-dissipative cyclical process (such as a non-dissipative Carnot cycle) must be reversible, so the extended Carnot theorem has already included the Carnot theorem, but not vice versa. The extended Carnot theorem is an extended foundation stone of thermodynamics (especially of modern thermodynamics) and a new starting point of the second law in the current 21st century. The extended Carnot theorem results in the establishment of a new field of non-dissipative and dissipative thermodynamics in modern thermodynamics [1].

Classical thermodynamics deals with simple systems with only spontaneous irreversible process, equilibrium systems and systems with reversible process [1]. The spontaneous process refers to the process occurring along such a direction that the process may automatically go on without other influences left. In the framework of classical thermodynamics, the second law is expressed as $dS_p = dS \geq 0$, where dS_p is the entropy change of the process, and dS is the entropy change of the system. The classical thermodynamics cannot deal with the multi-process complex system. This is because the complex system may contain both spontaneous process and non-spontaneous process. The non-spontaneous process is a process that takes place along a direction opposite to that of spontaneous process. The non-spontaneous process should be driven by the spontaneous process to occur [1,2]. A chemical reaction system including positive reaction and reverse reaction is an example of the multi-processes complex system [1]. The second law gave the criterion of $d_i S_1 < 0$, $d_i S_2 > 0$ and $d_i S \geq 0$ for such a system, where $d_i S_1$ is the entropy change for non-spontaneous process such as the reverse reaction, $d_i S_2$ is the entropy change of spontaneous process, and $d_i S$ is the global entropy change of the system. Such second law criterion is beyond the scope of classical thermodynamics. The concept of non-dissipation and dissipation is the core concept of modern

* Corresponding author.

E-mail address: xjl@ncepu.edu.cn (J. Xu).

Nomenclature

C	efficiency coefficient	ΔT^*	non-dimensional integration temperature difference
c	proportionality coefficient, K	ΔT_h^*	non-dimensional integration temperature difference in heating process
c_p	specific heat at constant pressure, J/(kg·K)	ΔT_c^*	non-dimensional integration temperature difference in cooling process
dS	entropy change of the system, J/K	W or W_{exp}	output work, W
dS_p	entropy change of the process, J/K	X	general thermodynamic force
En	dissipation for heat to power conversion, K·W		
En_h	dissipation for heat to power conversion in heating process, K·W		
En_c	dissipation for heat to power conversion in cooling process, K·W		
I	exergy destruction, W		
J	general thermodynamic flow		
L	phenomenological coefficient		
LMTD	logarithmic-mean-temperature-difference, K		
m	mass flow rate, kg/s		
P	pressure, Pa		
Q	heat transfer rate or heat load, W		
R	resistance ratio of heating process with respect to cooling process		
R_h	resistance for heat to power conversion in heating process, 1/(K·W)		
R_c	resistance for heat to power conversion in cooling process, 1/(K·W)		
r	$r = En_{h,l}/En_{h,s}$		
S	entropy, J/K		
T	temperature, K		
$T_{h,1}$	temperature of heat source fluid entering the heat engine, K		
$T_{h,2}$	temperature of heat source fluid leaving the heat engine, K		
$T_{h,3}$	temperature of working fluid entering the evaporator, K		
$T_{h,4}$	temperature of working fluid leaving the evaporator, K		
$T_{c,1}$	temperature of environment fluid entering the heat engine, K		
$T_{c,2}$	temperature of environment fluid leaving the heat engine, K		
$T_{c,3}$	temperature of working fluid entering the condenser, K		
$T_{c,4}$	temperature of working fluid leaving the condenser, K		
$T_{c,p}$	temperature of environment fluid at pinch point, K		
ΔT	integration temperature difference, K		
ΔT_h	integration temperature difference in heating process, K		
ΔT_c	integration temperature difference in cooling process, K		
		<i>Greek symbols</i>	
		η_{real}	actual thermal efficiency
		η_{carnot}	carnot efficiency
		ζ	dryness, J/kg·K ²
		<i>Subscripts</i>	
		c	cooling fluid or cooling process
		cr	critical point
		exp	expander
		h	heating fluid or heating process
		k, l, m	serial numbers
		l	latent heat evaporation
		pc	pseudo-critical point
		r	organic fluid
		s	sensible heat
		A–H	state points along ORC cycle
		A	heat carrier fluid entering the heat engine
		B	heat carrier fluid leaving the heat engine
		C	working fluid entering the evaporator
		D	working fluid leaving the evaporator
		E	working fluid entering the condenser
		F	working fluid leaving the condenser
		G	environment fluid (or say cooling fluid) entering the heat engine
		H	environment fluid (or say cooling fluid) leaving the heat engine
		A', G', I, I'	Points to form the enclosed area
		M	pseudo-critical point or bubble point of working fluid in the evaporator
		M'	heat source fluid point corresponding to point M for working fluid
		0	reference state
		1–4, 3'	state points along ORC

thermodynamics. For simple non-coupling system, “reversible” is identical to “non-dissipation”, and “irreversible” is identical to “dissipation”. However, for a multi-processes complex system, the terms of “non-dissipation” and “dissipation” should be used instead of “reversible” and “irreversible” [1,2]. For example, for the thermal coupling in a heat exchanger, a hot fluid enters the heat exchanger at $T_{h,1}$ and leaves the heat exchanger at $T_{h,2}$ ($T_{h,2} < T_{h,1}$), and a cold fluid enters the heat exchanger at $T_{c,1}$ and leaves the heat exchanger at $T_{c,2}$ ($T_{c,2} > T_{c,1}$). If the temperature difference between the hot and cold fluids is infinitely small, the heat transfer process approaches non-dissipation to reach maximum heat transfer efficiency, but this is an irreversible process because the hot fluid can heat the cold fluid but the cold fluid cannot heat the hot fluid.

When a system involving several dissipation processes, a flow of one process not only depends on the corresponding dissipation process, but also depends on other dissipation processes. The influence among different dissipation processes is called thermodynamic coupling. Therefore, a thermodynamic flow J_k is a function of all the thermodynamic forces X_i in the system:

$$J_k = J_k\{X_i\} \tag{1}$$

Taking several thermodynamic force $\{X_i\} = 0$ and thermodynamic flow $J_k\{X_i\} = 0$ as the reference point, Eq. (1) becomes

$$J_k\{X_i\} = J_k\{X_{l,0}\} + \sum_l \left(\frac{\partial J_k}{\partial X_l} \right)_0 X_l + \frac{1}{2} \sum_{l,m} \left(\frac{\partial^2 J_k}{\partial X_l \partial X_m} \right)_0 X_l X_m + \dots \tag{2}$$

If a system approaches the reference point, in which the thermodynamics forces are so small that the high power terms are negligible, then a linear phenomenological relation exists

$$J_k = \sum_l L_{kl} X_l \tag{3}$$

where $L_{kl} = \left(\frac{\partial J_k}{\partial X_l} \right)_0$. The phenomenological coefficients L_{kk} represent the relation between thermodynamic force X_k and corresponding thermodynamic flow J_k . Alternatively, L_{kl} represents coupling between different dissipation processes. Coefficients L_{kk} can be resistance for electric current flow, or thermal resistance for heat

transfer process [3]. Detailed description about the dissipative thermodynamics can be found in Refs. [1–5].

The dissipative thermodynamics has successfully dealt with problems such as the single-way cyclical reactions in linear regime and chemical oscillations in nonlinear regime [1]. Very few studies were reported on the heat engine analysis using the dissipative thermodynamics. Fig. 1 shows a general heat engine, which is an open system. Heat received from the heat source is Q_h . The heat source fluid enters the heat engine at the temperature $T_{h,1}$ and leaves the heat engine at the temperature $T_{h,2}$. Heat dissipated to the environment is Q_c . The cooling fluid enters the heat engine at the temperature $T_{c,1}$ and leaves the heat engine at the temperature $T_{c,2}$. The first law efficiency is

$$\eta_{real} = 1 - \frac{Q_c}{Q_h} \quad (4)$$

The second law efficiency (also called the exergy efficiency) is defined as

$$\eta_{II} = 1 - \frac{\text{destroyed exergy}}{\text{supplied exergy}} \quad (5)$$

It is noted that the Carnot efficiency is $\eta_{Carnot} = 1 - T_0/T$, where T_0 is the environment temperature and T is the heat source temperature. The Carnot efficiency specifies the maximum thermal efficiency limit. The Carnot efficiency is for general heat engines and there are other similar efficiency expressions such as endoreversible efficiency. By comparing η_{real} and η_{Carnot} , one understands the approaching degree of the real thermal efficiency to the Carnot efficiency. For a heat engine, once the state parameters at various state points are known, one yields the thermal efficiency and the exergy efficiency. The higher η_{real} and η_{II} , the better performance of a heat engine is. However, the efficiencies defined in Eqs. (4) and (5) cannot tell us how to increase efficiencies. This is because a heat engine performance not only depends on the state parameters at various state points, but also depends on the roadmaps of the process. From modern thermodynamics point of view, for a heat engine shown in Fig. 1, thermal couplings exist between heat source and heat engine, as well as between heat engine and cooling fluid. Beside, coupling among different processes (heating and cooling process) should be treated. Such dissipation process (roadmaps of the process) should be dealt with by introducing the concept of thermodynamics flow and thermodynamics force.

The objective of this paper is to develop an actual thermal efficiency expression for general heat engines. The developed thermal

efficiency can also be called the hybrid thermal efficiency. This is because the efficiency deduction uses both the energy conservation principle and the dissipation caused exergy destructions. The major contribution of this paper is to establish the relationship between the thermodynamic flow (Q_h and Q_c) and the dissipations of heating and cooling processes. The dissipation strongly relies on the heat transfer roadmaps, which can be considered as the integration effect. The resistance of heat to power conversion is defined as R_h for heating process and R_c for cooling process. Finally, the real thermal efficiency is expressed as a function of R , which is the ratio of R_h divided by R_c . Holding the real thermal efficiency, one knows how to improve the heat engine performance. The actual thermal efficiency is suitable for general heat engines such as coal-fired power plant and renewable energy driving thermal plant. As an application example, the real thermal efficiency theory guides us the selection of working fluids for Organic Rankine Cycles (ORCs). The influence of critical temperatures of working fluids on ORCs was paid great attention. Critical temperature of the working fluid affects the heat transfer roadmaps to determine dissipations in heating and cooling processes. The system performance is strongly dependent on the fluid critical temperatures.

2. The heat engine model

Fig. 1 shows a general heat engine model. A heat exchanger receives heat from heat source with heating load as Q_h . This heat exchanger is called as the heating heat exchanger. Any heat engine should dissipate a part of heat load to environment. The heat rejected to environment is recorded as Q_c . The heat exchanger dissipating heat to environment is called the cooling heat exchanger. In such a model, the heat engine is a system, which interacts with the heat source recorded as the heating side coupling. The heat engine also interacts with the cooling medium as the cooling side coupling. Any heat engine may contain other components such as pump or turbine. The actual thermal efficiency development starts from using the first law efficiency based on the energy conservation principle ($W = Q_h - Q_c$, where W is the work output). It is necessary to deal with the heating side and cooling side couplings and link the two couplings together. This does not mean the exergy destruction contributions by pump or turbine are not important. The contributions of these components influence the state parameters at various state points to alter the effect of heat transfer roadmaps on the system thermal performance. In one word, the pump or turbine contributions are reflected in the model, implicitly.

3. Theoretical model for actual thermal efficiencies

According to the heat engine model shown in Fig. 1, the heating side coupling and cooling side coupling are dealt with first. Then, linking the two thermal couplings yields the actual thermal efficiency expression.

For heating process: The thermal coupling between heat source and working fluid of the heat engine is considered here. Fig. 2a plots T - Q curves of the two-fluids in a counter-flow heating heat exchanger, in which four state points are marked by parameters of heat flow and temperature. Curves AB and CD represent heat transfer roadmaps for heat carrier fluid of heat source and working fluid of the heat engine, respectively. The enclosed red area (ABCD) is

$$En_h = \int_0^{Q_h} \Delta T dQ = \int_0^{Q_h} (T_{\text{heat source}} - T_{\text{working fluid}}) dQ \quad (6)$$

where $T_{\text{heat source}}$ is the heat carrier fluid temperature of the heat source. The exergy destruction during the heat transfer process is [6]

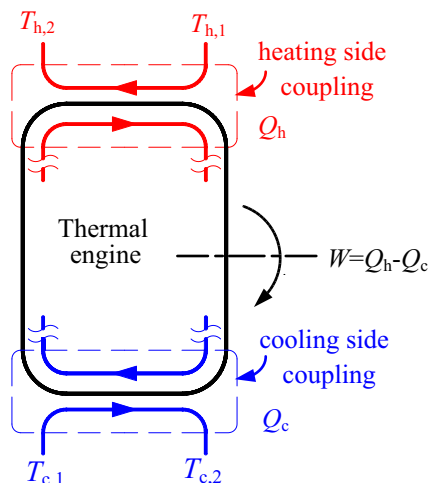


Fig. 1. The heat engine model used in this study.

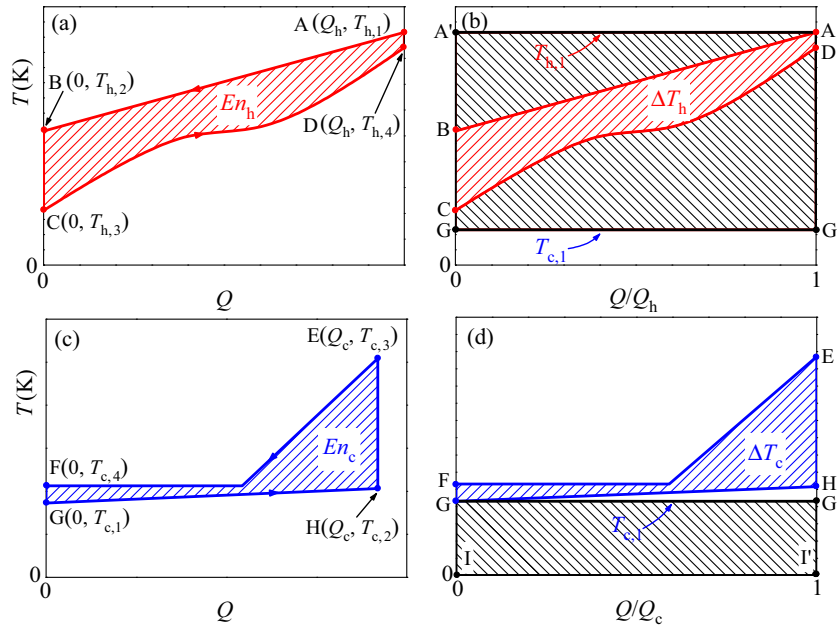


Fig. 2. Definition of dissipation for heat to power conversion (En), integration temperature difference (ΔT), non-dimensional integration temperature difference (ΔT^*) for heating and cooling processes (a: En_h for heating process, b: red area ABCD is ΔT_h , ΔT_h^* is the red area ABCD divided by the rectangular area AA'GG', for heating process, c: En_c for cooling process, d: blue area EFGH is ΔT_c , ΔT_c^* is the blue area EFGH divided by the rectangular area GG'I'I', for cooling process). (For interpretation of the references to color in this figure legend, the reader is referred to the web version of this article.)

$$I = T_0 \int_0^{Q_h} \frac{(T_{\text{heat source}} - T_{\text{working fluid}})}{T_{\text{heat source}} T_{\text{working fluid}}} dQ \quad (7)$$

where T_0 is the referenced environment temperature, which can be $T_{c,1}$ for environmental fluid entering the cooling heat exchanger. Our previous paper proved that the enclosed area given in Eq. (6) is directly proportional to the exergy destruction expressed in Eq. (7) [6]. Our recent experiment also verified that this conclusion is correct [7]. The units of En_h and I are K-W and W, respectively. If one writes $En_h = c \cdot I$, the proportionality coefficient c has the temperature unit of K. This means that c depends on the heat source temperature level $T_{h,1}$. Our studies in Ref. [6] did show this trend. Physically, the exergy destruction represents loss of energy quality, or say loss of available energy. Thus, En_h in Eq. (6) is called the dissipation for heat to power conversion in the heating process.

Fig. 2b shows T - Q/Q_h , in which the horizontal axis ranges from 0 to 1 for the non-dimensional heat flow. The enclosed red area (ABCD) represents the integration temperature difference ΔT_h :

$$\Delta T_h = \frac{En_h}{Q_h} \quad (8)$$

ΔT_h quantifies how better the thermal coupling between heat source and working fluid is for heat to power conversion, referenced by the total heat flow Q_h . Further, the non-dimensional integration temperature difference ΔT_h^* is introduced as

$$\Delta T_h^* = \frac{\Delta T_h}{T_{h,1} - T_{c,1}} = \frac{En_h}{(T_{h,1} - T_{c,1})Q_h} \quad (9)$$

ΔT_h^* is the enclosed red area (ABCD) divided by the rectangular area (AA'GG') in Fig. 2b, quantifying how better the heat transfer process is for heat to power conversion in heating process, referenced by driving temperature difference between heat source and environment ($T_{h,1} - T_{c,1}$), and heat flow Q_h . It can be understood as the dissipation from heat source to heat engine (En_h), at the cost of ($T_{h,1} - T_{c,1}$) and Q_h .

Eq. (9) is rewritten as

$$Q_h = \frac{En_h}{(T_{h,1} - T_{c,1})\Delta T_h^*} \quad (10)$$

According to dissipative thermodynamics, Q_h is the “thermodynamics flow”, En_h is the “thermodynamic force”, $\frac{1}{(T_{h,1} - T_{c,1})\Delta T_h^*}$ is the “phenomenological coefficient”. Eq. (10) establishes the connection between Q_h , En_h , $T_{h,1} - T_{c,1}$ and ΔT_h^* .

For cooling process: Thermal coupling between working fluid of heat engine and cooling medium (such as water or air) also influences system performance. Fig. 2c shows T - Q curves of the two streams of counter-flow cooling heat exchanger. The curve EF represents heat transfer roadmap of working fluid of heat engine, and GH represents the heat transfer roadmap of the cooling medium. Depending on the fluid state in the cooling heat exchanger, the curve EF can be linearly changed, or includes two sub-sections of a superheated vapor flow section and an isothermal condensation section. But this does not influence the general treatment of the cooling process. Fig. 2d shows T - Q/Q_c curves, in which dimensionless heat flow is used.

Similar to the deduction in heating process, En_c (EFGH in Fig. 2c) and ΔT_c (EFGH in Fig. 2d) for cooling process are

$$En_c = \int_0^{Q_c} \Delta T dQ = \int_0^{Q_c} (T_{\text{working fluid}} - T_{\text{environment fluid}}) dQ \quad (11)$$

$$\Delta T_c = \frac{En_c}{Q_c} \quad (12)$$

$$\Delta T_c^* = \frac{\Delta T_c}{T_{c,1} - 0} = \frac{En_c}{T_{c,1}Q_c} \quad (13)$$

In Eq. (13), $T_{c,1} - 0$ means the maximum cooling capability at an environment fluid temperature of $T_{c,1}$ entering the heat engine related to the absolute 0 K. $T_{c,1} - 0$ is the driving temperature difference between $T_{c,1}$ of an environment fluid entering a heat engine and the thermodynamic absolute 0 K, in which 0 K is defined as the

minimum temperature in the nature world that can be approached. The kinetic energy is zero at 0 K. The deduction of absolute 0 K was performed by Kelvin and it can be found in Wang et al. [1]. ΔT_c^* is indicated by the blue area (EFGH) divided by the black rectangular area (GG'I'I) in Fig. 2d. Eq. (13) is written as

$$Q_c = \frac{En_c}{T_{c,1}\Delta T_c^*} \quad (14)$$

According to the dissipative thermodynamics, Q_c is the “thermodynamic flow”, En_c is the “thermodynamic force”, $\frac{1}{T_{c,1}\Delta T_c^*}$ is the “phenomenological coefficient”.

Coupling between heating and cooling processes: Thermal efficiency of a heat engine is defined as

$$\eta_{real} = 1 - \frac{Q_c}{Q_h} \quad (15)$$

Substituting Eqs. (10) and (14) into Eq. (15), η_{real} is

$$\eta_{real} = 1 - \frac{\eta_{Carnot} R}{1 - \eta_{Carnot}} \quad (16)$$

where η_{Carnot} is the Carnot efficiency with $T_{h,1}$ as the heat source temperature and $T_{c,1}$ as the environment temperature:

$$\eta_{Carnot} = 1 - \frac{T_{c,1}}{T_{h,1}} \quad (17)$$

R is the ratio of resistance of heating process R_h divided by that of cooling process R_c , for heat to power conversion:

$$R = \frac{R_h}{R_c} \quad (18)$$

where R_h and R_c are

$$R_h = \frac{\Delta T_h^*}{En_h} = \frac{1}{(T_{h,1} - T_{c,1})Q_h}, \quad R_c = \frac{\Delta T_c^*}{En_c} = \frac{1}{T_{c,1}Q_c} \quad (19)$$

Eqs. (16)(19) give the actual thermal efficiency of a heat engine, η_{real} , relating to the Carnot efficiency by a new efficiency coefficient C as

$$\eta_{real} = C\eta_{Carnot} \quad (20)$$

C characterizes the degree at which real thermal efficiency deviates from Carnot efficiency. It is a function of Carnot efficiency and resistance ratio:

$$C = f(\eta_{Carnot}, R) = \frac{1}{\eta_{Carnot}} - \frac{R}{1 - \eta_{Carnot}} \quad (21)$$

It is convenient to calculate actual thermal efficiency by Eqs. (20) and (21), in which R is computed by Eqs. (18) and (19). The theoretical development tells us how to raise the actual thermal efficiency. Physically, the decrease of resistance ratio of heating process related to cooling process, R , is a general solution to increase the efficiency coefficient C , yielding the actual thermal efficiency improvement. This requires the decrease of the resistance of heating process, R_h , and/or increase of the resistance of cooling process, R_c . It is noted that both R_h and R_c are the resistances for heat to power conversion, not for heat transfer analysis. En_h and En_c have the unit of $K \cdot W$, identical to entransy unit. The entransy concept was described in Prof. Guo's series papers and it is useful for heat exchanger optimization [8–12]. Han et al. [13] used entransy concept to develop a Carnot engine model.

The actual thermal efficiency expressed by Eqs. (17)(21) does not contain the loss of work potentials of other components such as pump and turbine of heat engines. This is because the deduction of η_{real} used the first law efficiency (see Eq. (15) for the energy conservation principle). Based on the modern thermodynamics framework, this paper treated Q_h as the thermodynamic flow, and

established the relationship between the thermodynamic flow and the thermodynamic force for the heating process (see Eq. (10)). Similar procedure was performed for the cooling process (see Eq. (14)). Thus, the loss of work potentials of pump and turbine does not appear in the real thermal efficiency expression explicitly, but it influences the real thermal efficiency implicitly. The loss of work potentials of these components may affect the state parameters of the cycle to change the coupling between heat source and heat engine, as well as between heat engine and cooling medium.

4. Application of the actual thermal efficiency theory to the analysis of Organic Rankine Cycles (ORCs)

ORC converts low grade energy (such as flue gas discharged from boiler) and renewable energy (such as solar thermal energy and geothermal energy) into useful power or electricity. Various low grade energy sources exist in the industry. In north part of China, natural gas fired boilers, instead of coal fired boilers, are strongly recommended to supply heat for residents in winter season, for the environment protection purpose. Usually, flue gas with its temperature of 140–150 °C is directly discharged to the environment. ORC can recover the waste heat of flue gas into electricity. For such application, the outlet flue gas temperature after the waste heat recovery can be 80–90 °C. The temperature limit of 80–90 °C approaches the dew point temperature of the flue gas, below which the corrosion of heat exchanger occurs due to the condensed water from vapor in the flue gas. Considering flow rate and temperature difference (for example, from inlet temperature of 150 °C to outlet temperature of 85 °C) of the flue gas, the waste heat in ~ MW scale can be recovered by ORC, for a single natural gas boiler. The ~100 kW scale electricity can be generated, which is of benefit to the heat supply industry.

Eqs. (17)(21) are general expressions for the actual thermal efficiency. In this section, how the theoretical work guides the analysis of Organic Rankine Cycles (ORCs) is demonstrated. A key issue is to select suitable working fluids. There are many articles on the selection of working fluids [6,14–19]. General conclusion about this has not been reached at this stage. The following reasons cause the scattered data on the selection of working fluids: (1) Heat sources: There are various heat sources such as flue gas, water-vapor steam, solar thermal energy and geothermal energy. Different heat sources may require different working fluids. Some authors selected fluids assuming the maximum organic fluid temperature in ORC equal to the heat source temperature [20], deviating from the practical condition. The fluid selection shall couple ORC with heat source. Not only the heat carrier fluid temperature entering ORC, but also the heat carrier fluid temperature leaving ORC and mass flow rate should be involved in the fluid selection. (2) Physical properties: Physical properties such as latent heat of evaporation, density, specific heat, viscous and thermal conductivity of organic fluids influence ORC performance [21]. (3) Operation parameters: The operation parameters of organic fluids at various state points of ORC influence the cycle performance. Some authors assumed the saturation vapor at the expander inlet to determine the “best” fluid [20]. Recent experimental study showed that the superheating vapor can prevent the expander from cavitation [7]. (4) Objective parameters: Most of studies determined the “best” fluid based on the maximum thermal efficiency criterion. Alternatively, some investigators selected the fluid based on multi objective parameters such as thermal efficiency and system cost or size [22,23]. Different criteria yield different results of working fluids.

We use the newly developed actual thermal efficiency to explain the effect of critical temperatures of organic fluids on the

ORC performance. Fig. 3a shows an ORC, including a heating heat exchanger (HHE), an expander, a cooling heat exchanger (CHE) and a pump. For a general ORC, the heat source can be flue gas, solar thermal energy, geothermal energy or vapor, etc. [24–27]. Any environment fluid can dissipate heat to environment. In this study, the flue gas, as a kind of waste heat, was used as the heat source, water was the cooling medium. W_{exp} represents the output work of expander, m_h and m_c represent the mass flow rate of flue gas and water, respectively. Fig. 3b shows the T - S diagram. Serial numbers 1–4 represent the state points along the ORC, and $T_{c,p}$ is the pinch temperature of water in condenser.

In this study, the flue gas enters and leaves ORC at $T_{h,1} = 423.15$ K (150 °C) for supercritical condition, $T_{h,1} = 448.15$ K (175 °C) for subcritical condition and $T_{h,2} = 358.15$ K (85 °C) for both cases, respectively. The heating load is fixed as $Q_h = 1000$ kW (1 MW). Specific heat of the flue gas is constant. The temperature difference at the narrowed location in T - Q curve is called the pinch temperature, which should be larger than 5 K. For the cooling side coupling, the cooling water enters ORC at $T_{c,1} = 293.15$ K (20 °C). The mass flow rate of cooling water is selected based on the criterion that pinch temperature difference in the cooling heat exchanger equals to 5 K. Isentropic efficiencies of expander and circulating pump are 0.75.

4.1. Effect of critical temperatures of organic fluids on super-critical pressure ORCs

In this section, the effect of critical temperatures of organic fluids on super-critical pressure ORCs is explored. The organic fluids of R218, R32, propylene, R134a, R1234ze and isobutane are used. The critical temperatures are gradually increased from R218 to isobutane (see Table 1 for the major properties of these fluids). For each fluid, the state parameters at various points of the cycle are determined according to the method described in Yu et al. [6]. A major step is to determine an optimal operation pressure at the expander inlet (P_1). A set of pressures are tried. Each pressure corresponds to a specific actual thermal efficiency η_{real} . Thus, a specific pressure P_1 is obtained to have the maximum η_{real} , also corresponding to the maximum work due to the fixed Q_h . The optimal pressure P_1 is about 0.3 MPa higher than the fluid critical pressure T_{cr} . Thus, $P_1 = P_{cr} + 0.3$ MPa for all the fluids. For each fluid, the actual thermal efficiency and related parameters are determined based on the section of theoretical model for actual thermal efficiencies. En_h and En_c are the integration terms:

$$En_h = \int_0^{Q_h} \Delta T dQ \approx \sum_{i=1}^N (T_{heat\ source} - T_{working\ fluid})_i \Delta Q \quad (22)$$

$$En_c = \int_0^{Q_c} \Delta T dQ \approx \sum_{i=1}^N (T_{working\ fluid} - T_{environment\ fluid})_i \Delta Q \quad (23)$$

where $\Delta Q = Q_h/N$ in Eq. (22) and $\Delta Q = Q_c/N$ in Eq. (23), N is the section number that sub-divides Q_h or Q_c . When N is sufficiently large, for example, when it is larger than 1000, the computation has enough accuracy. Eqs. (22) and (23) are the numerical integration forms for En_h and En_c to simplify the calculation. They are correct if one assumes quasi-constant temperature difference ΔT within a narrow range of ΔQ .

After obtaining En_h , En_c , ΔT_h , ΔT_c , ΔT_h^* , ΔT_c^* , R_h , R_c , R , C and η_{real} for each fluid, these parameters are plotted versus T_{cr} in Fig. 4, noting that each data point corresponds to a specific organic fluid with a given T_{cr} . With increases of T_{cr} , dissipation for heat to power conversion En , integration temperature difference ΔT , and non-dimensional integration temperature difference ΔT^* are decreased, for heating and cooling processes. It should be noted that R_h for heating process is inverse to $(T_{h,1} - T_{c,1})Q_h$, in which both $(T_{h,1} - T_{c,1})$ and Q_h are not changed. Thus, R_h is constant for different organic fluids. However, R_c for the cooling process, is increased by increasing T_{cr} (see Fig. 4d), yielding decreased resistance ratio R of heating process with respect to cooling process to increase efficiency coefficient C and real thermal efficiency η_{real} (see Fig. 4e and f).

Fig. 5 explains parameter variations shown in Fig. 4, noting that $T_{h,1} = 423.15$ K. The distance from $T_{h,1}$ to T_{pc} (pseudo-critical temperature of organic fluid) influences roadmaps in T - Q curve to affect thermal couplings between heat source and ORC, as well as ORC and cooling fluid. Fig. 5a and b compares specific heat variations for R218 with lower $T_{cr} = 345.02$ K and for R1234ze with higher $T_{cr} = 382.51$ K. The distance from T_{pc} to $T_{h,1}$ is shorter for R1234ze than that for R218 (see Fig. 5a and b). Specific heat (c_p) variations are divided into two parts: the increased CM part before T_{pc} and decreased MD part beyond T_{pc} . Such c_p distributions yield T - Q curves shown in Fig. 5c and d. Because specific heat for flue gas is constant, AB shows linear curve. But strong c_p variations for super-critical pressure fluid yields curved CD. Dissipation for heat to power conversion in heating process, En_h , represented by enclosed ABCD area, is sub-divided into two areas: black $M'BCM$ area and red $AM'MD$ area. The CD curve has slope of

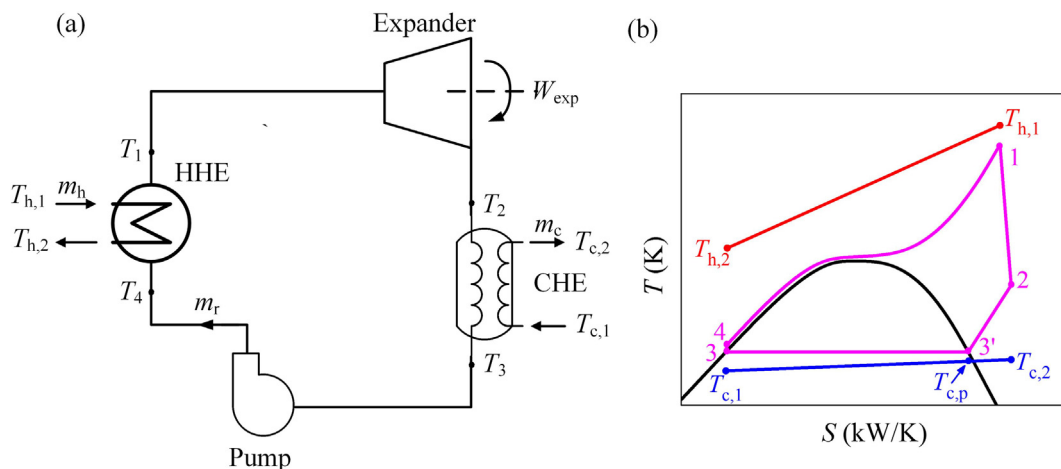


Fig. 3. The ORC configuration (a) and The T - S diagram (b).

Table 1
Organic fluid database in this study.

No.	Working fluid	Formula	T_c (K)	P_c (MPa)	ξ (J/kg·K ²)	Toxicity	Flammability
1	R218	C3F8	345.02	2.64	0.708	Non	Extremely
2	R32	CH2F2	351.26	5.78	-0.560	Non	Extremely
3	Propylene	C3H6	364.21	4.56	-4.183	Non	Extremely
4	R134a	C2H2F4	374.21	4.06	-0.961	Low	Non
5	R227ea	C3HF7	374.9	2.93	0.575	/	/
6	R1234ze	C3H2F4	382.52	3.64	-0.338	Non	Highly
7	R12	CCl2F2	385.12	4.14	-0.969	Low	Non
8	Perfluorobutane	C4F10	386.33	2.32	1.314	/	/
9	RC318	C4F8	388.38	2.78	0.907	Low	Non
10	R124	C2HClF4	395.43	3.62	-0.138	Low	Non
11	Trifluoroiodomethane	CF3I	396.44	3.95	-0.727	High	Non
12	R236fa	C3H2F6	398.07	3.20	0.511	Low	Non
13	Isobutane	C4H10	407.81	3.63	-0.419	Low	Extremely
14	R142b	C2H3ClF2	410.26	4.06	-0.703	Non	Extremely
15	R236ea	C3H2F6	412.44	3.50	0.584	/	/
16	Isobutene	C4H8	418.09	4.01	-0.805	Non	Extremely
17	R114	C2Cl2F4	418.83	3.26	0.405	Low	Non
18	Butene	C4H8	419.29	4.01	-1.005	Non	Extremely
19	R245fa	C3H3F5	427.16	3.65	0.32	Low	Non
20	Transbutene	C4H8	428.61	4.03	-0.873	/	Extremely
21	Neopentane	C5H12	433.74	3.20	1.127	Low	Extremely
22	cis-Butene	C4H8	435.75	4.23	-1.137	Non	Extremely
23	R245ca	C3H3F5	447.57	3.93	0.516	/	/
24	R21	CHCl2F	451.48	5.18	-1.244	Non	Non
25	R123	C2HCl2F3	456.83	3.66	0.16	High	Non
26	R365mfc	C4H5F5	460	3.27	1.040	/	/
27	Isopentane	C5H12	460.35	3.38	1.131	Low	Extremely
28	R11	CCl3F	471.11	4.41	-0.410	Low	Non
29	R113	C2Cl3F3	487.21	3.39	0.515	Low	Non
30	Acetone	C3H6O	508.1	4.70	-1.048	Low	Highly
31	Cyclopentane	C5H10	511.69	4.52	-0.156	Low	Highly
32	Cyclohexane	C6H12	553.64	4.08	1.341	High	Highly
33	Dimethyl carbonate	C3H6O3	557.38	4.84	0.6017	Non	Highly
34	Benzene	C6H6	562.02	4.91	0.237	High	Highly
35	Toluene	C7H8	591.75	4.13	1.076	High	Highly

Note: ξ represents the dryness of each fluid.

$$\frac{\partial T}{\partial Q} = \frac{1}{m_r c_{p,r}} \quad (24)$$

where m_r is mass flow rate of organic fluid and $c_{p,r}$ is specific heat of organic fluid. The CM part is protruding to approach AB due to decreased slope of $\frac{\partial T}{\partial Q}$ with increased $c_{p,r}$. Alternatively, the MD part is concaved to recede AB due to increased slope with decreased $c_{p,r}$. The two regimes are interfaced at M having $\left. \frac{\partial^2 T}{\partial Q^2} \right|_M = 0$.

Decrease of dissipation for heat to power conversion in heating process means to decrease the enclosed $ABCD$ area. Indeed, fluid such as R1234ze having higher critical temperature, elongates protruding CM part but shortens concaved MD part to improve the thermal coupling between heat source and organic fluid, compared with lower critical temperature fluid such as R218 (see Fig. 5c and d). The blue $EFGH$ area represents En_c for heat to power conversion in cooling process, in which EF and GH represent T - Q curves for organic fluid and cooling water, respectively. Higher critical temperature fluid also improves the thermal coupling between ORC and cooling fluid, by significantly shortening superheating vapor flow section in condenser (the cooling heat exchanger operates at sub-critical pressure). Fig. 5e and f shows the T - S curves. The enclosed pink area represents useful work, which is larger with R1234ze than that with R218. Point D is closer to the critical point for R1234ze than that for R218. The four state points A , B , C and D are identical in Fig. 5c and d, but the roadmaps from C to D are different to show the effect of heat transfer roadmaps on heat to power conversion.

In summary, critical temperature of organic fluid is critical to determine cycle performance. Higher critical temperature fluid not only elongates specific heat increase part to improve thermal

coupling between heat source and organic fluid, but also shortens superheating vapor flow section in condenser to improve thermal coupling between ORC and cooling fluid, which are the mechanism to increase real thermal efficiencies.

4.2. Effect of critical temperatures of organic fluids on sub-critical pressure ORCs

Here, the effect of critical temperatures of organic fluids on ORCs is investigated. Running parameters such as $T_{h,2}$, Q_h , T_c , pinch temperature requirement, and isentropic efficiencies of expander and pump are identical to those for the supercritical pressure ORC cases. Heat engine operates at sub-critical pressures with evaporation (phase change heat transfer) in evaporator and condensation in condenser. The optimal operation pressure P_1 at the expander inlet was iteratively searched to maximize the thermal efficiency according to Xu et al. [14]. Thirty one organic fluids are involved. With critical temperatures from low to high, fluids are listed as follows: R227ea, R1234ze, R12, perfluorobutane, RC318, R124, trifluoroiodomethane, R236fa, isobutane, R142b, R236ea, isobutene, R114, butene, R245fa, transbutene, neopentane, cis-butene, R245ca, R21, R123, R365mfc, isopentane, R11, R113, acetone, cyclopentane, cyclohexane, Dimethyl carbonate, benzene and toluene. R227ea and toluene have critical temperatures of 374.9 K and 591.75 K, respectively (see Table 1 for properties).

Fig. 6 demonstrates En_h , En_c , ΔT_h , ΔT_c , ΔT_h^* , ΔT_c^* , R_h , R_c , R , C and η_{real} versus T_{cr} . Again, each data point corresponds to a specific fluid having a known critical temperature. $T_{h,1}$ is marked in Fig. 6a. For heating process, dissipation for heat to power conversion, En_h , integration temperature difference, ΔT_h , and

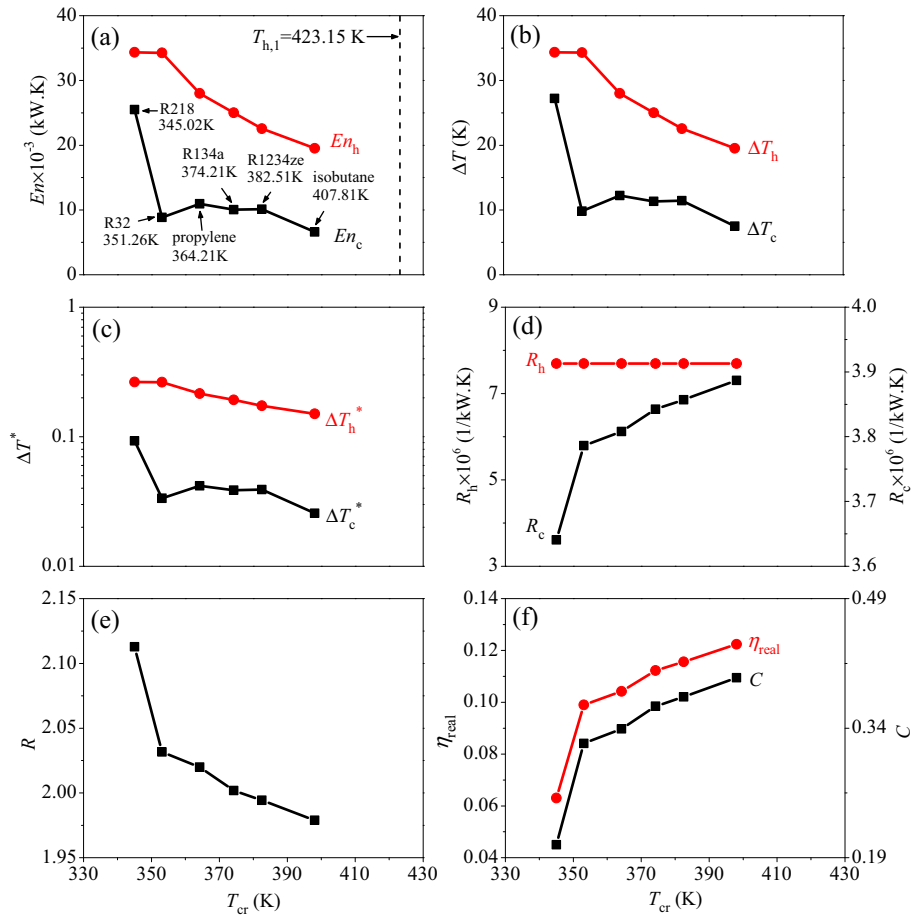


Fig. 4. Parameters of trans-critical pressure ORC versus T_{cr} with six organic fluids.

non-dimensional integration temperature difference, ΔT_h^* , are sharply decreased to minimum point, followed by a gentle increase trend (see red curves in Fig. 6a–c). For cooling process, En_c , ΔT_c and ΔT_c^* behave slight oscillating but do not change too much. Because heating load Q_h and temperature difference between heat source and heat sink ($T_{h,1} - T_{c,1}$) are given values, resistances for heat to power conversion in heating process, R_h , are not changed for different organic fluids. Resistances for heat to power conversion in cooling process, R_c , show inverse trend of En_h , ΔT_h and ΔT_h^* in heating process (see Fig. 6d). The resistance ratio R is sharply decreased to a minimum point, followed by slight variance. Thus, efficiency coefficient C and real thermal efficiencies η_{real} are increased and then almost keep constant, by increasing critical temperatures T_{cr} .

Figs. 7 and 8 explain data trends in Fig. 6. T - Q curves are shown for heating and cooling processes with R227ea, R236fa, trans-butene and cyclopentane. In evaporator, organic fluid undergoes a single-phase liquid heating section, represented by black area $En_{h,s}$, and an isothermal evaporation flow section, represented by red area $En_{h,l}$. For fluids with low critical temperatures such as R227ea and R236fa, the strict pinch temperature difference of 5 K is not reached. The enclosed $ABCD$ area, representing dissipation for heat to power conversion in heating process, is approximated as a parallelogram with its area scaled as $|BC| \times Q_h = (T_{h,2} - T_{h,3})Q_h$ (see Fig. 7a and b). Fig. 7c shows that when fluid critical temperature approaches heat source temperature $T_{h,1}$, pinch temperature occurs at the junction between liquid flow part and isothermal evaporation part, under which $ABCD$ area recedes to a triangle with its area scaled as $0.5|BC| \times Q_h =$

$0.5(T_{h,2} - T_{h,3})Q_h$, because pinch temperature is significantly lower than $|BC|$. The latent heat evaporation contributes less dissipation for heat to power conversion (see red area in Fig. 7c).

When fluid critical temperature is beyond heat source temperature (see Fig. 7d), the pinch temperature shifts to evaporator entrance. The $ABCD$ area, including black $En_{h,s}$ and red $En_{h,l}$ parts, is also equivalent to a triangle area scaled as $0.5(T_{h,2} - T_{h,3})Q_h$, providing $|AD|$ not deviating from $|BC|$ too much and small pinch temperature. This explains why thermal efficiencies are not sensitive to critical temperatures when critical temperatures are higher than heat source temperature.

Fig. 8 illustrates T - S curves for the four fluids. For fluids having critical temperatures lower than heat source temperature, the pink area, representing useful work, is below the heat source line AB . The pink area is lifting to approach AB line by increasing T_{cr} , until a quasi-triangle cycle is reached with $T_{cr} \rightarrow T_{h,1}$, under which the fluid critical point is close to point A (see Fig. 8a–c). Fig. 8d shows the case when fluid critical temperature is higher than heat source temperature at point A . The fluid T - S envelope is intercrossed with the heat source line AB , but the pink area shows smaller difference with that shown in Fig. 8c.

For subcritical pressure ORCs, Figs. 6–8 show that when the heat source line AB is fixed, fluid critical temperatures strongly influence heat transfer roadmaps to yield different dissipation for heat to power conversion for heating process. Low critical temperature fluids fatten the enclosed area of T - Q curves to suppress thermal efficiencies. If fluid critical temperatures approach or are beyond heat source temperature, the enclosed area of T - Q curves for heating process become slim to enhance thermal efficiencies.

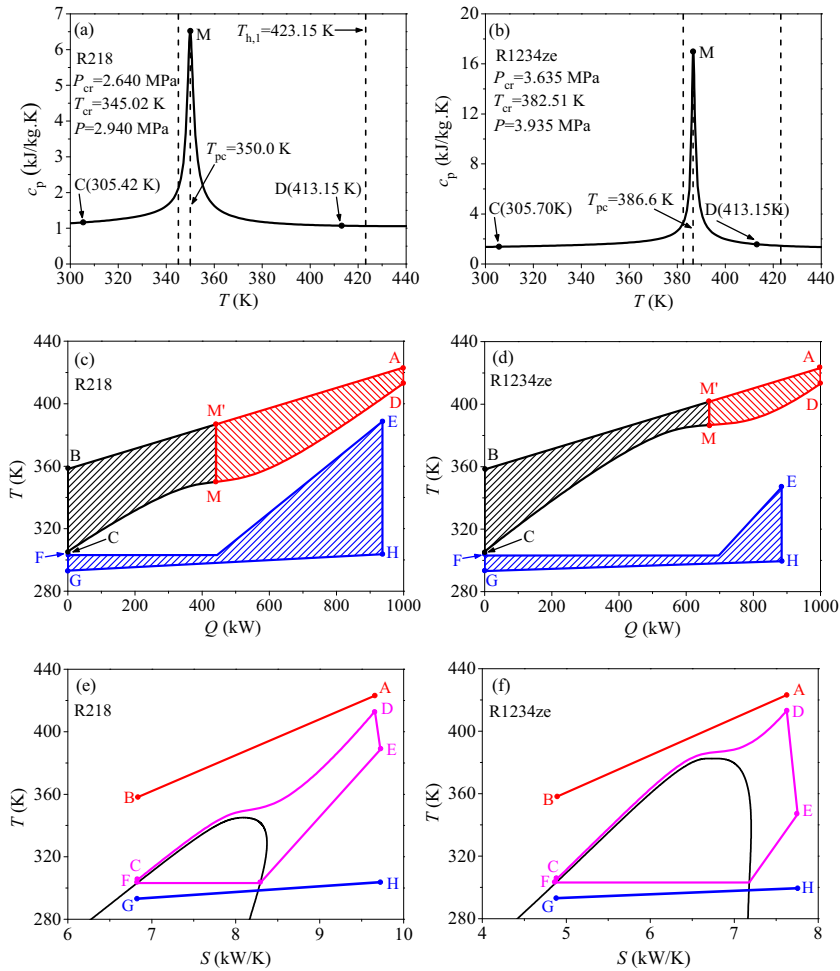


Fig. 5. Heat transfer roadmaps effect on trans-critical pressure ORCs by comparing R218 and R1234ze.

The above analysis is based on the pinch temperature difference of 5 K in both evaporator and condenser. The pinch temperature limit influences the system thermal efficiency. Generally, a smaller pinch temperature limit results in a higher thermal efficiency because sufficient heat transfer area is provided. The pinch temperature limit is set to be in the range of 5–20 K, in which the lower limit of 5 K was used by Chen et al. [20], Heberle and Brüggemann [28], Wang et al. [29] and He et al. [30]. Effect of pinch temperature on actual thermal efficiencies is shown in Fig. 9. The three pinch temperatures of 5 K, 10 K and 15 K were used. The efficiency curves display two regions: a sharp increase region before the maximum efficiency point and a slight decrease region beyond the maximum efficiency point. The pinch temperature does not affect the change trend of efficiency curves. The increased pinch temperatures slightly shift the maximum efficiency points to lower critical temperatures of organic fluids. The pinch temperature does not apparently affect the selection of organic fluids. The objective of this paper is to demonstrate how the newly developed theory is used for the fluid selection. The optimization among various parameters such as thermal efficiency and component size or cost will be shown in the future.

Fig. 9 shows actual thermal efficiencies dependent on critical temperatures of organic fluids. Saleh et al. [31] noted that fluids with lower critical temperatures such as R143a or R152a were preferable. Liu et al. [32] showed that the thermal efficiency is a weak function of critical temperatures. Kuo et al. [33] and Mikielewicz and Mikielewicz [34] proposed the Jakob number as the

criterion number for fluid selections. Aljundi [35] found the strong functionality between thermal efficiencies and fluid critical temperatures. This study found the strong connection between thermal efficiencies and fluid critical temperatures. Different from the findings of Aljundi [35], this study identified a sharp efficiency increase region before maximum efficiency point (sensitive region) and a slight decrease region beyond maximum efficiency point (not sensitive region). For ORC operation, the not sensitive region is recommended because it includes the maximum efficiency point followed by the very gentle variation of thermal efficiencies. The heat carrier fluid temperature entering ORC is marked as $T_{h,1}$ in Fig. 9 (also called the heat source temperature). The maximum efficiency point is weakly dependent on the pinch temperatures. For the pinch temperature of 5–15 K, organic fluids having critical temperatures in the range of $(T_{h,1} - 40 \text{ K}, T_{h,1} + 100 \text{ K})$ are recommended. The not sensitive efficiency region expands the fluid candidates, which is not reported previously. This criterion for organic fluid selection is proposed from the thermal efficiency point of view. For practical utilization, a specific fluid also should be high thermal stability, low environment impact and safety.

4.3. Comment on the actual thermal efficiency

There are two efficiencies in the literature: the first law thermal efficiency written as $\eta = W/Q_h$, and the exergy efficiency defined as used exergy divided by available exergy. The former is written based on the energy conservation principle and has nothing to

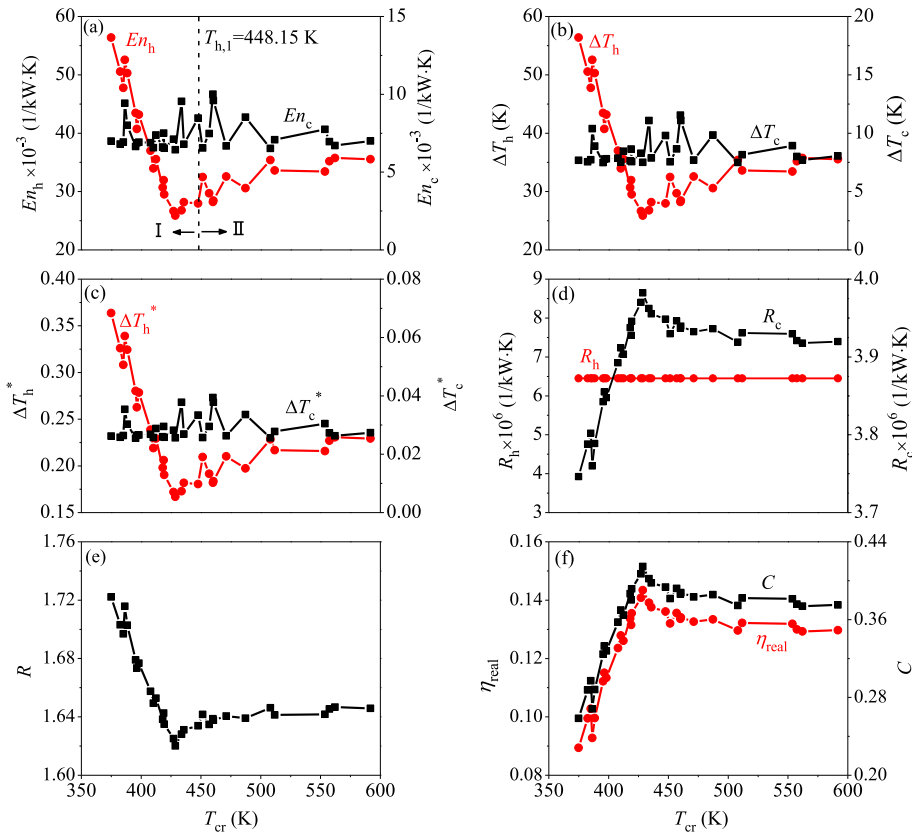


Fig. 6. Parameters of sub-critical pressure ORCs versus T_{cr} . (from left to right, the fluids are: R227ea, R1234ze, R12, perfluorobutane, RC318, R124, trifluoroiodomethane, R236fa, isobutane, R142b, R236ea, isobutene, R114, butene, R245fa, transbutene, neopentane, cis-butene, R245ca, R21, R123, R365mfc, isopentane, R11, R113, acetone, cyclopentane, cyclohexane, Dimethyl carbonate, benzene and toluene).

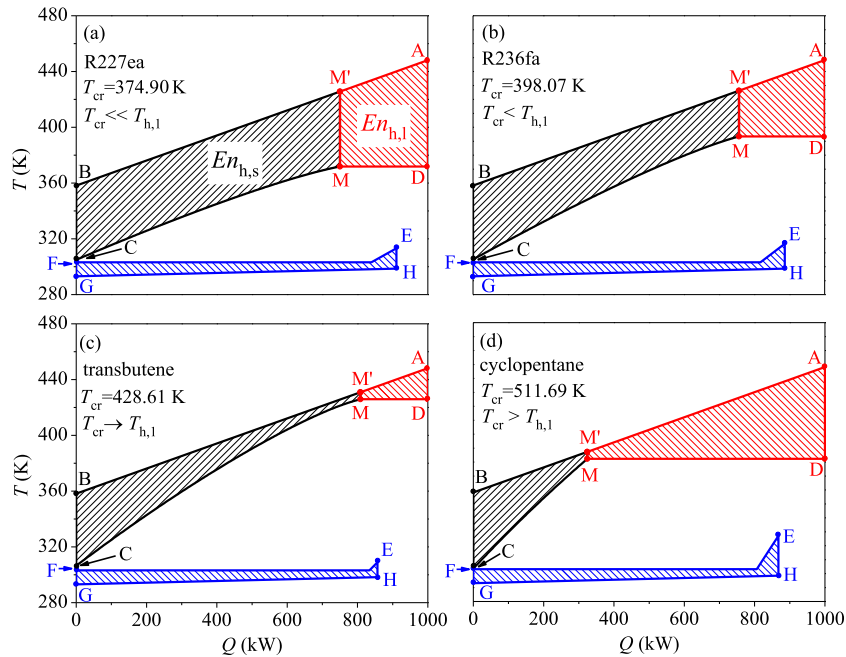


Fig. 7. Effect of heat transfer roadmaps on sub-critical pressure ORCs with R227ea, R236fa, transbutene and cyclopentane.

do with the loss of energy quality. The later is also called the second law efficiency [36]. Here, a purely theoretical expression of actual thermal efficiency is developed. Because it synthesizes energy conservation and loss of energy quality, it is also called a hybrid efficiency. The actual thermal efficiency tells us that, no

matter how complex a heat engine is, the engine should reach a lower resistance ratio of heating process related to cooling process to have a higher thermal efficiency. A lower resistance for heat to power conversion in heating process, and/or a larger resistance for heat to power conversion in cooling process, is necessary.

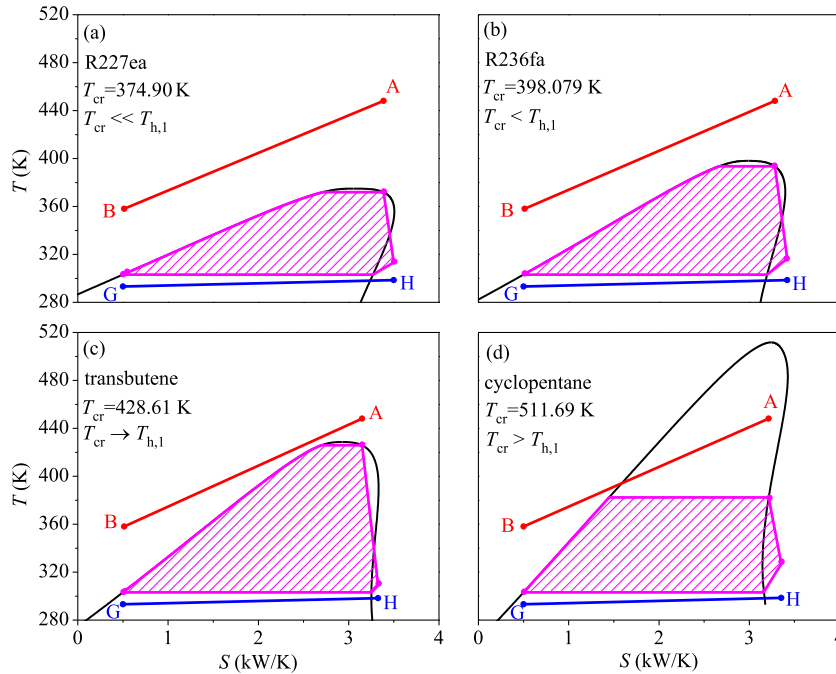


Fig. 8. T-S curves for four working fluids of R227ea, R236fa, transbutene and cyclopentane.

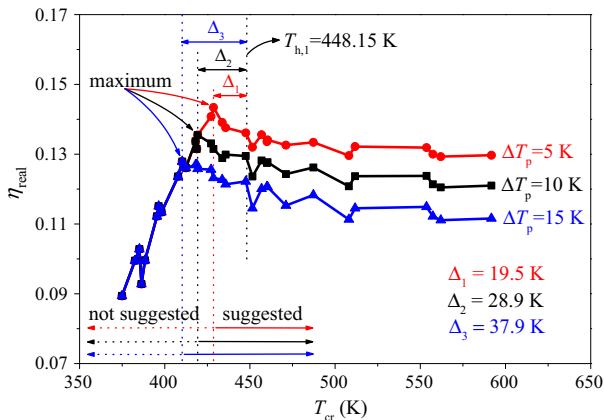


Fig. 9. Effect of pinch temperature on η_{real} .

Checking dissipations for heat to power conversion in heating and cooling processes, one can see how better the thermal couplings between heat source, heat engine and environment fluid are.

In our theoretical development, integration temperature difference and non-dimensional integration temperature difference are involved. In heat transfer textbooks, the logarithmic-mean-temperature-difference (LMTD) has been widely used [37]. Referring a heat exchanger shown in Fig. 2a, LMTD is

$$\Delta T_{\log-m} = \frac{\Delta T_{\max} - \Delta T_{\min}}{\ln\left(\frac{\Delta T_{\max}}{\Delta T_{\min}}\right)} \quad (25)$$

where

$$\begin{aligned} \Delta T_{\max} &= \max[(T_{h,1} - T_{h,4}), (T_{h,2} - T_{h,3})] \\ \Delta T_{\min} &= \min[(T_{h,1} - T_{h,4}), (T_{h,2} - T_{h,3})] \end{aligned} \quad (26)$$

Eqs. (25) and (26) only consider temperatures at state points of A, B, C and D. LMTD is suitable for heat transfer analysis. It does not

contain *roadmap integration effect* thus it has nothing to do with loss of energy quality. Alternatively, integration temperature difference reflects integration effect. The enclosed area of T-Q curves is directly proportional to exergy destruction. Thus, it is not only suitable for heat transfer analysis, but also suitable for heat to power conversion analysis. Non-dimensional integration temperature difference links the roadmap integration effect referenced as the system driving temperature difference between heat source and environment fluid for heating process, or referenced as the maximum cooling capability for cooling process. Thus, integration temperature difference, or non-dimensional integration temperature difference, helps us to see how better the thermal couplings between heat source, heat engine and cooling fluid are.

The actual thermal efficiency theory provides guidance for design and operation of thermal plant, which can be coal-fired power plant [38–40], renewable energy driving thermal plant [41–43], biomass plant [44–46], etc. Improving the performance of these plants is helpful to raise energy utilization efficiency and reduce carbon dioxide (CO₂) emission. The following aspects are discussed.

Coupling between heat source and heat engine: The present work treats the coupling between heat source and heat engine, from both energy balance and loss of energy quality point of view. The heat carrier fluid of heat source, temperatures entering and leaving heat engine, specific heat variations even latent heat influence the T-Q curve in heating heat exchanger, which can be evaluated by the present model.

Design and operation parameters of heat engine: The present work guides the selection of working fluid to well match the heat source. It also helps to pick out suitable operation parameters such as pressures and temperatures of working fluid in the cycle. The physical properties and running parameters determine T-Q curves in both heating and cooling heat exchangers to affect the engine efficiency and work output.

Cooling effect on the heat engine: Most heat engines use water or air to dissipate heat to environment. Cooling effect influences the resistance for heat to power conversion. For example, when a

heat engine uses air as the cooling medium, the so-called energy penalty exists [47,48]. The problem such as how to decrease the energy penalty can be evaluated by the present theory.

5. Conclusions

An actual thermal efficiency for heat engines is developed. Concepts of “thermodynamics flow” and “thermodynamics force”, in modern thermodynamics, are used for theoretical analysis. The enclosed area of T - Q curves in heat exchangers are quantified to represent exergy loss during heat transfer process, as the dissipation for heat to power conversion in heating and cooling heat exchangers. Integration temperature difference reflects roadmap integration effect to consider the loss of energy quality. Non-dimensional integration temperature difference is the integration temperature difference scaled by the temperature difference between heat source and working fluid for heating process, or scaled by the cooling capability represented by environment fluid temperature for cooling process. The efficiency coefficient C quantifies the degree at which actual thermal efficiency deviates from Carnot efficiency. C is a linear function of the resistance ratio of heating process related to cooling process for heat to power conversion.

The theory successfully explains effect of critical temperatures of organic fluids on supercritical pressure ORCs. Higher critical temperature fluids elongate the specific heat increase part but shorten the specific heat decrease part to create a slim enclosed area of T - Q curves in heating heat exchanger. Thus, the heat transfer induced dissipation is decreased to improve thermal efficiencies.

For sub-critical pressure ORCs, when the critical temperature of working fluid approaches or is beyond the heat source temperature, a small pinch temperature is formed to generate a triangle area, which can be half of that with ultra-low critical temperature fluid. Critical temperatures are critical to influence the working fluid roadmap to affect the cycle performance.

Conflict of interest

The authors declare no competing financial interests.

Acknowledgements

The authors thank for the funding support from Natural Science Foundation of China with contract numbers of 51210011 and 51436004.

References

- [1] J.T. Wang, *Modern Thermodynamics – Based on the Extended Carnot Theorem*, first ed., Springer, Berlin Heidelberg, 2011.
- [2] J.T. Wang, Modern thermodynamics – new concepts based on the second law of thermodynamics, *Progr. Nat. Sci.* 19 (2009) 125–135.
- [3] L. Onsager, Reciprocal relations in irreversible process, *Phys. Rev.* 37 (1931) 405–426.
- [4] X.F. Shen, G. Hu, L. Jiang, *Theory of Dissipative Structures*, Shanghai People's Publisher, 1987 (in Chinese).
- [5] I. Prigogine, R. Lefever, *Theory of Dissipative Structures*, Vieweg, Teubner, Verlagm, 1973.
- [6] C. Yu, J.L. Xu, Y.S. Sun, Trans-critical pressure Organic Rankine Cycle (ORC) analysis based on the integrated-average temperature difference in evaporators, *Appl. Therm. Eng.* 88 (5) (2015) 2–13.
- [7] X.F. Yang, J.L. Xu, Z. Miao, J.H. Zou, F.L. Qi, The definition of non-dimensional integration temperature difference and its effect on Organic Rankine Cycle, *Appl. Energy* 167 (2016) 17–33.
- [8] Z.Y. Guo, H.Y. Zhu, X.G. Liang, Entransy – a physical quantity describing heat transfer ability, *Int. J. Heat Mass Transf.* 50 (2007) 2545–2556.
- [9] Z.Y. Guo, X.B. Liu, W.Q. Tao, R.K. Shah, Effectiveness – thermal resistance method for heat exchanger design and analysis, *Int. J. Heat Mass Transf.* 53 (2010) 2877–2884.
- [10] Q. Chen, K.D. Yang, M.R. Wang, N. Pan, Z.Y. Guo, A new approach to analysis and optimization of evaporative cooling system I: theory, *Energy* 35 (6) (2010) 2448–2454.
- [11] X.T. Cheng, X.G. Liang, Z.Y. Guo, Entransy decrease principle of heat transfer in an isolated system, *Chin. Sci. Bull.* 56 (9) (2011) 847–854.
- [12] Q. Chen, X.G. Liang, Z.Y. Guo, Entransy theory for the optimization of heat transfer – a review and update, *Int. J. Heat Mass Transf.* 63 (2013) 65–81.
- [13] Y. Han, D.B. Wang, C.C. Zhang, Y.J. Zhu, The entransy degeneration and entransy loss equations for the generalized irreversible Carnot engine system, *Int. J. Heat Mass Transf.* 106 (2017) 895–970.
- [14] J.L. Xu, C. Yu, Critical temperature criterion for selection of working fluids for subcritical pressure Organic Rankine Cycles, *Energy* 74 (1) (2014) 719–733.
- [15] J.L. Xu, C. Liu, Effect of the critical temperature of organic fluids on supercritical pressure Organic Rankine Cycles, *Energy* 63 (15) (2013) 109–122.
- [16] J. Vivian, G. Manente, A. Lazzaretto, A general framework to select working fluid and configuration of ORCs for low-to-medium temperature heat sources, *Appl. Energy* 156 (15) (2015) 727–746.
- [17] A. Pezzuolo, A. Benato, A. Stoppato, A. Mirandola, The ORC-PD: a versatile tool for fluid selection and Organic Rankine Cycle unit design, *Energy* 102 (1) (2016) 605–620.
- [18] H. Yu, X. Feng, Y. Wang, A new pinch based method for simultaneous selection of working fluid and operating conditions in an ORC (Organic Rankine Cycle) recovering waste heat, *Energy* 90 (1) (2015) 36–46.
- [19] K.A. Barse, M.D. Mann, Maximizing ORC performance with optimal match of working fluid with system design, *Appl. Therm. Eng.* 100 (5) (2016) 11–19.
- [20] Q.C. Chen, J.L. Xu, H.X. Chen, A new design method for Organic Rankine Cycles with constraint of inlet and outlet heat carrier fluid temperatures coupling with the heat source, *Appl. Energy* 98 (2012) 562–573.
- [21] K. Rahbar, S. Mahmoud, R.K. Al-Dadah, N. Moazami, S.A. Mirhadizadeh, Review of organic Rankine cycle for small-scale applications, *Energy Convers. Manage.* 134 (2017) 135–155.
- [22] A. Toffolo, A. Lazzaretto, G. Manente, M. Paci, A multi-criteria approach for the optimal selection of working fluid and design parameters in Organic Rankine Cycle systems, *Appl. Energy* 121 (2014) 219–232.
- [23] Y.Q. Feng, T.C. Hung, Y.N. Zhang, B.X. Li, J.F. Yang, Y. Shi, Performance comparison of low-grade ORCs (Organic Rankine Cycles) using R245fa, pentane and their mixtures based on the thermoeconomic multi-objective optimization and decision makings, *Energy* 93 (2015) 2018–2029.
- [24] M. Wei, X. Zhao, L. Fu, S. Zhang, Performance study and application of new coal-fired boiler flue gas heat recovery system, *Appl. Energy* 188 (2017) 121–129.
- [25] J. Besong, R. Taccani, M.D. Lucia, D. Micheli, G. Toniato, Development and experimental characterization of a small scale solar powered Organic Rankine Cycle (ORC), *Energy Proc.* 101 (2016) 504–511.
- [26] X.H. Liu, Y.F. Zhang, J. Shen, System performance optimization of ORC-based geo-plant with R245fa under different geothermal water inlet temperatures, *Geothermics* 66 (2017) 134–142.
- [27] K. Braimakis, S. Karellas, Integrated thermoeconomic optimization of standard and regenerative ORC for different heat source types and capacities, *Energy* 121 (15) (2017) 570–598.
- [28] F. Heberle, D. Brüggemann, Exergy based fluid selection for a geothermal Organic Rankine Cycle for combined heat and power generation, *Appl. Therm. Eng.* 30 (2010) 1326–1332.
- [29] X. Wang, X.M. Liu, C.H. Zhang, Parametric optimization and range analysis of Organic Rankine Cycle for binary-cycle geothermal plant, *Energy Convers. Manage.* 80 (2014) 256–265.
- [30] C. He, C. Liu, H. Gao, H. Xie, Y.R. Li, S.Y. Wu, J.L. Xu, The optimal evaporation temperature and working fluids for subcritical organic Rankine cycle, *Energy* 38 (2012) 136–143.
- [31] B. Saleh, G. Koglbauer, M. Wendland, J. Fischer, Working fluids for low-temperature organic Rankine cycles, *Energy* 32 (2007) 1210–1221.
- [32] B.T. Liu, K.H. Chien, C.C. Wang, Effect of working fluids on organic Rankine cycle for waste heat recovery, *Energy* 29 (2004) 1207–1217.
- [33] C.R. Kuo, S.W. Hsu, K.H. Chang, C.C. Wang, Analysis of a 50 kW organic Rankine cycle system, *Energy* 36 (2011) 5877–5885.
- [34] D. Mikielewicz, J. Mikielewicz, A thermodynamic criterion for selection of working fluid for subcritical and supercritical domestic micro CHP, *Appl. Therm. Eng.* 30 (2010) 2357–2362.
- [35] I.H. Aljundi, Effect of dry hydrocarbons and critical point temperature on the efficiencies of organic Rankine cycle, *Renew Energy* 36 (2011) 1196–1202.
- [36] Y.A. Cengel, M.A. Boles, *Thermodynamics – An Engineering Approach*, fifth ed., 1998.
- [37] J.P. Holman, *Heat Transfer*, 10th ed., New York, 2010.
- [38] C. Xu, G. Xu, S.F. Zhao, L.Y. Zhou, Y.P. Yang, D.K. Zhang, An improved configuration of lignite pre-drying using a supplementary steam cycle in a lignite fired supercritical power plant, *Appl. Energy* 160 (2015) 882–891.
- [39] C. Xu, G. Xu, S.F. Zhao, W. Dong, L.Y. Zhou, Y.P. Yang, A theoretical investigation of energy efficiency improvement by coal pre-drying in coal fired power plants, *Energy Convers. Manage.* 122 (15) (2016) 580–588.
- [40] G. Xu, C. Xu, Y.P. Yang, Y.X. Fang, Y.Y. Li, X.N. Song, A novel flue gas waste heat recovery system for coal-fired ultra-supercritical power plants, *Appl. Therm. Eng.* 67 (2014) 240–249.

- [41] R.R. Zhai, M.M. Zhao, K.Y. Tan, Y.P. Yang, Optimizing operation of a solar-aided coal-fired power system based on the solar contribution evaluation method, *Appl. Energy* 146 (2015) 328–334.
- [42] H. Gökgedik, M. Yürüsoy, A. Keçebaş, Improvement potential of a real geothermal power plant using advanced exergy analysis, *Energy* 112 (2016) 254–263.
- [43] M.R. Rodríguez-Sánchez, A. Sánchez-González, P.A. González-Gómez, C. Marugán-Cruz, D. Santana, Thermodynamic and economic assessment of a new generation of subcritical and supercritical solar power towers, *Energy* 118 (2017) 534–544.
- [44] C.Q. Dong, Y.P. Yang, R. Yang, J.J. Zhang, Numerical modeling of the gasification based biomass co-firing in a 600 MW pulverized coal boiler, *Appl. Energy* 87 (2010) 2834–2838.
- [45] H. Athari, S. Soltani, S.M.S. Mahmoudi, M.A. Rosen, T. Morosuk, Exergoeconomic analysis of a biomass post-firing combined-cycle power plant, *Energy* 77 (1) (2014) 553–561.
- [46] T. Muche, C. Höge, O. Renner, R. Pohl, Profitability of participation in control reserve market for biomass-fueled combined heat and power plants, *Renew Energy* 90 (2016) 62–76.
- [47] X.Z. Du, H.M. Hu, Y.Q. Shen, L.J. Yang, Y.P. Yang, Reduced order analysis of flow and heat transfer for air-cooled condenser of power generating unit, *Appl. Therm. Eng.* 51 (2013) 383–392.
- [48] L. Chen, L.J. Yang, X.Z. Du, Y.P. Yang, A novel layout of air-cooled condensers to improve thermo-flow performances, *Appl. Energy* 165 (2016) 244–259.